
CHAPTER 4: COMPLEX VOLTAMMETRIC RESPONSE

In this chapter, the bistable $\text{Pt}|\text{H}_2\text{SO}_4|\text{H}_2$ system is investigated. In contrast to the forthcoming chapters 5-8, the investigations are focused mainly on temporal phenomena rather than spatiotemporal dynamics. More precisely, the dynamics of the $\text{Pt}|\text{H}_2\text{SO}_4|\text{H}_2$ system when subjected to a periodic forcing will be studied. The periodic forcing employed has the form of a voltage ramp, and thus the instabilities occurring during *cyclic voltammetric* experiments are discussed.

4.1 INTRODUCTION

In cyclic voltammetry experiments the current/voltage response begins to repeat itself after a finite number of voltage cycles, i.e., it settles down to a stationary profile which is invariant in time. Thus, the current/time trace is periodic and possesses the same period as the imposed voltage scan. This conventional response represents a so-called 'period-1 cyclic voltammogram (CV)'.

A high-order periodic CV is a CV in which the period of the current response is a multiple of the period of the applied voltage. For example, in a period-2 CV the current/time trace repeats itself after two periods of the external voltage. Such high-order periodic CVs as well as aperiodic CVs, in which the current never settles down to a periodic behavior, were reported by Schell and coworkers for the oxidation of several organic molecules, such as methanol, ethanol, and propanol, on Pt and Pd electrodes in both acidic and alkaline media [152-159]. The complex voltammetric responses were obtained within a certain range of the positive turning point of the applied voltage over wide ranges of other control parameters, such as concentrations of the educts, electrolyte conductivity, or rotation rate of the electrode. Another example of such complex voltammetric behavior has recently been observed by Dolata and Kawczynski [160] during the anodic dissolution of copper in concentrated sulfuric acid.

Schell and co-workers suggest that a nonlinear feedback mechanism, which involves the reaction of PtOH with the intermediate PtCO as well as the conversion of PtOH to Pt oxides, is crucial for the occurrence of complex voltammetric responses. The unusual cyclic voltammetric behavior is then believed to be the result of the interplay between the periodically forced applied potential (i.e., the potential cycling) and the specific nonlinearities of the electrochemical reactions with the organic compound [156, 157].

In this chapter very similar phenomena observed during hydrogen oxidation in the Pt/H₂SO₄/H₂ system [161, 162] are presented. In this system, the hypotheses that any carbon containing intermediate is essential for the mechanism causing the complex voltammetric behavior can be excluded *a priori*. In the following a general mechanism for the occurrence of the high-order periodic and aperiodic cyclic voltammograms is presented. The mechanism only depends on properties of the electrode material (Pt and Pd) and is independent of the specific oxidation reactions under investigation. It thus should hold for both the hydrogen

oxidation reaction and the oxidation of organic substances. The chapter is structured as follows. Section 4.1 deals with the experimental results and the discussion on the main experimental findings. In section 4.2, the mechanism is translated into a mathematical model and simulations are presented. The general discussion in section 4.3 focuses on a comparison between simulations and experimental results. Finally, the main findings are summarized in the concluding section 4.4.

4.2 EXPERIMENTS

4.2.1 MAIN FINDINGS

Figure 4.1 shows four CVs of the $\text{Pt}|\text{H}_2\text{SO}_4|\text{H}_2$ system which were obtained for four different values of the positive turning point (U_2) and otherwise identical experimental conditions.

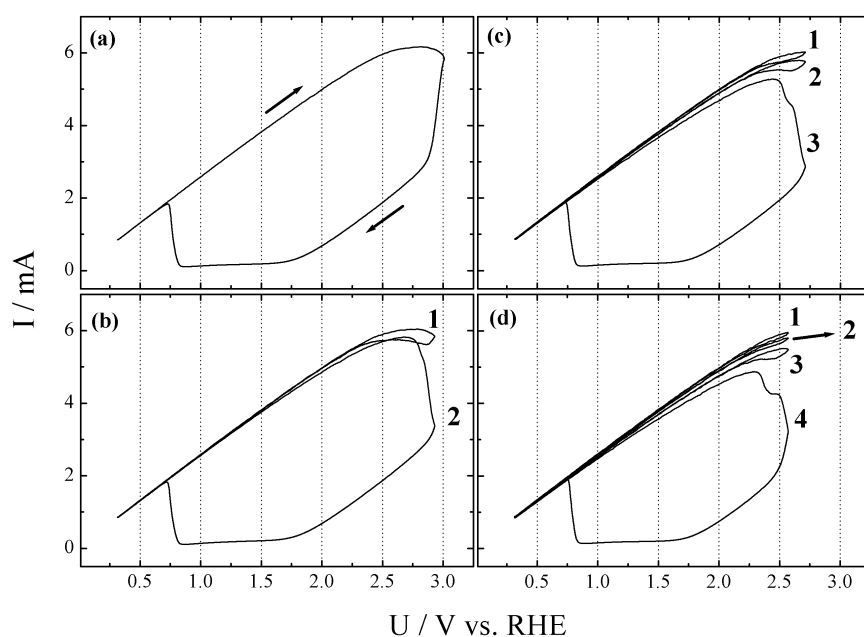


Figure 4.1: Cyclic voltammograms of the $\text{Pt}|\text{H}_2\text{SO}_4|\text{H}_2$ system at different positive turning points of the external voltage (U_2): (a) 3.01 V, (b) 2.93 V, (c) 2.71 V, and (d) 2.57 V. Remaining parameters: Negative turning point $U_1 = 0.31$ V, scan rate 0.1 V s^{-1} , electrolyte: 0.875 mM H_2SO_4 , H_2 saturated; uncompensated resistance: $410 \pm 5 \text{ } \Omega$; $\omega = 20 \text{ Hz}$. The anodic turning point was decreased stepwise, i.e., the order of measurements is (a) – (d). The numbers indicate the sequence in which cyclic voltammograms occur.

The I/U curve depicted in Figure 4.1 (a) was obtained for the most positive value of U_2 and can be rationalized as follows. The initially linear increase of the current, I , with increasing applied voltage, U , reflects the high electrolyte resistance⁶, R_Ω , which determines the form of the I/U curve at low overpotential. As already discussed in chapter 2, the potential-independent current plateau at larger values of U indicates mass transport limitation, whereas the current decrease close to the positive turning point is due to the oxidation of the Pt surface according to step (iv) [87, 88],



For this comparatively high electrolyte resistance of the experiments, the decrease in current leads to an increase in the true electrode potential, which becomes so positive close to the positive turning point that oxygen evolution occurs. Hence, the linearly decreasing current on the negative scan results from oxygen evolution. Once platinum oxide is formed, the reverse processes of step (iv) occur at much higher (negative) overpotential, causing the large hysteresis between the forward and backward scans in the CV.

Upon decreasing U_2 one would intuitively expect that from a threshold potential on, hydrogen is oxidized on the forward and backward scans with approximately the same rates since the potential at which Pt is oxidized is not reached anymore. However, this behavior is only found for considerably lower values of U_2 . For intermediate values of U_2 , high-order periodic CVs are observed which are composed of a different number of these two limiting CVs. Examples of period-2, 3 and 4 CVs, which emerged after decreasing U_2 in steps of 0.02 V, are shown in Figure 4.1 (b) – (d). For simplicity, in the following, a I/U cycle in which the H_2 oxidation current remains high throughout the cycle and thus exhibits only a small hysteresis around the positive turning point will be denoted an ‘S-cycle’. In the same way, the one during which oxide formation takes place leading to a large hysteresis in the oxidation current will be termed an ‘L-cycle’. In the period-2 CV (Figure 4.1 (b)), where S- and L-cycles alternate; such a period-2 response is termed an SL-state. In Figure 4.1 plates (c) and (d), two and three S-cycles, respectively, are periodically followed by an L-cycle. These complex CVs are thus examples of period-3 S^2L - and period-4 S^3L -states.

A closer examination of the S-cycles in Figures 4.1 (c) and (d) shows that they are not identical but differ slightly in the maximal current density close to U_2 . When plotting the current as a function of time, as done in Figure 4.2 (b) for the S^3L -state of Figure 4.1 (d), it becomes apparent that the maximum current decreases for successive S-cycles (cycles 1-3), is minimal for an L-cycle (cycle 4). It is reset to its maximal value for the first S-cycle after an L-cycle (cycle 5), from where the slow decrease starts again. Note that in Figure 4.2 and all successive figures time has been normalized to the period of a voltage cycle, T_u . For clarity, Figure 4.2 (a) shows the externally imposed voltage, U , as a function of time.

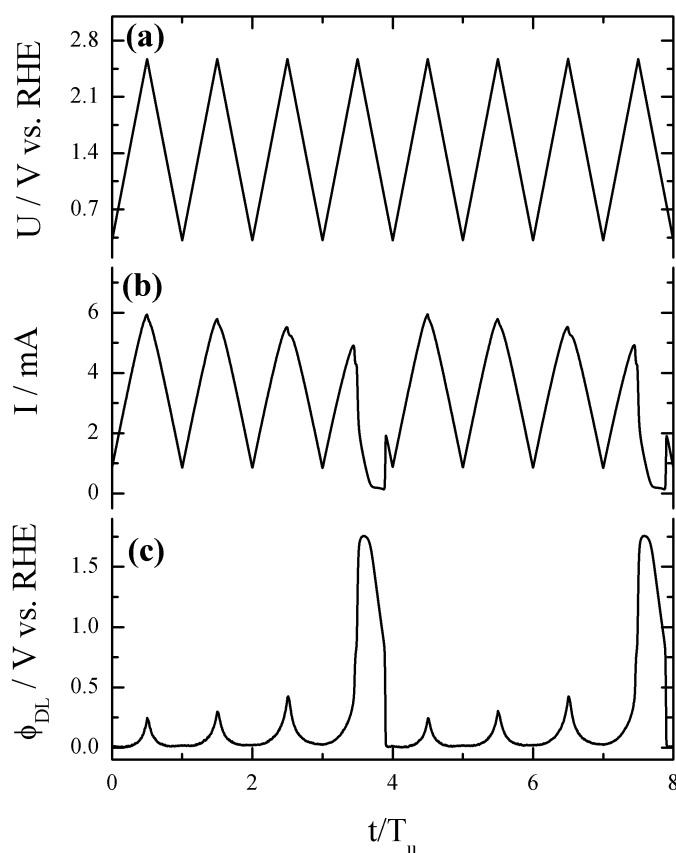


Figure 4.2: (a) Externally applied voltage, U , (b) current, I , and (c) true electrode potential, ϕ_{DL} , as a function of time (measured in units of the period of the applied voltage T_u) for the period-4 CV shown in Figure 4.1(d). (ϕ_{DL} was calculated according to $U = \phi_{DL} - R_{\Omega} I$, for $R_{\Omega} = 410 \Omega$.)

Since the experiments were conducted under potential control and in an electrolyte with low ionic strength, lower values of the current density imply that the true electrode

⁶ Since in the experiments presented in this chapter the external RE was used, the ohmic drop through the electrolyte is given in terms of R_{Ω} since it is equal to R_u .

potential, ϕ_{DL} , takes on larger values. Thus, although U_2 is kept constant during the cycling, the upper limit of the true electrode potential, $\phi_{DL,max}$, differs in the individual cycles of a high-order periodic CV. This can be seen in Figure 4.2 (c), in which ϕ_{DL} is plotted vs. time. ϕ_{DL} was calculated from $U - IR_{\Omega} = \phi_{DL}$, where R_{Ω} is the uncompensated cell resistance. In fact, such a freedom in the true electrode potential can be further illustrated by plotting the data shown above in Figure 4.1 (b) and (c) in terms of ϕ_{DL} as depicted in Figure 4.3. Here it is possible to realize what was just explained in the previous figure, i.e., although U_2 was kept constant (= 2.93 V in (a) and 2.17 V in (b)), $\phi_{DL,max}$ reaches values of 0.66 and 1.78 V (cycles 1 and 2, respectively, in Figure 4.3 (a)) and 0.34, 0.46, and 1.76 V (cycles 1, 2 and 3, respectively, in Figure 4.3 (b)).

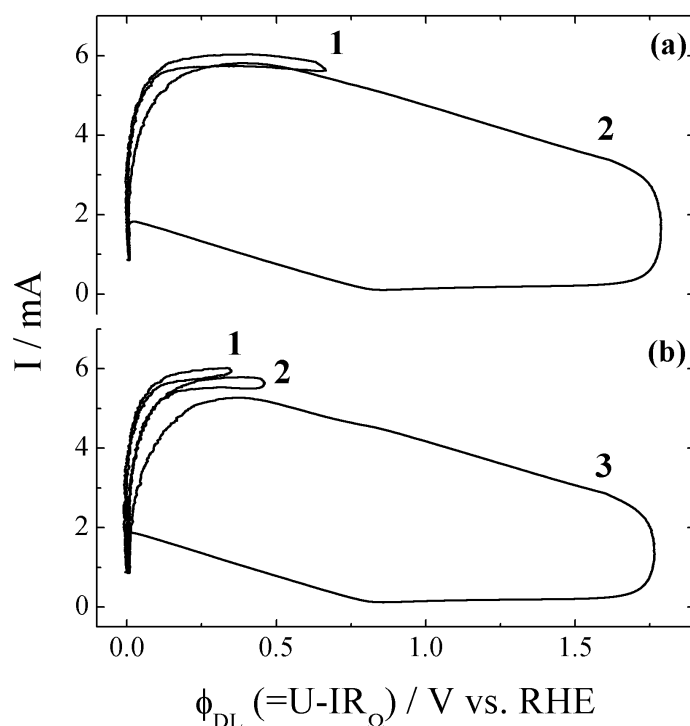


Figure 4.3: I/ϕ_{DL} potentiodynamic profiles for two different values of U_2 : (a) 2.93, and (b) 2.17 V. (a) and (b) were obtained from Figures 4.1 (b) and (c), respectively, after subtracting the IR_{Ω} contribution from U .

Owing to the drastic differences of $\phi_{DL,max}$ for an S- and an L-cycle as well as its distinct values for each S-cycles within one full period of the CV, $\phi_{DL,max}$ will be taken as variable for the further characterization of the complex voltammetric responses. In the bifurcation diagram depicted in Figure 4.4, $\phi_{DL,max}$ values are plotted against the value of the positive turning point, U_2 , which was decreased from 3.03 V in steps of 0.02 V. Up to $U_2 =$

2.95 V only period-1 CVs with large hysteresis cycles (L-cycles) existed. In an L-cycle, $\phi_{DL,max}$ takes on a value of about 1.82 V (squares in Figure 4.4). When the U_2 value is further decreased, the period-2 response appears at $U_2 = 2.93$ V giving rise to another branch of $\phi_{DL,max}$ (circles in Figure 4.4). The coexistence of these two branches evidences period-2 LS responses like the one shown in Figure 4.1 (b). A third and a fourth branch appear at $U_2 = 2.73$ V and $U_2 = 2.59$ V, respectively, manifesting the transition into a period-3 (S^2L)-state, and a period-4 (S^3L)-state.

Two trends become apparent: First, the higher the period of the CV, the smaller the range of anodic turning points, U_2 , in which the respective cycle exists. Since in the experiments U_2 was changed in steps of 0.02 V, it cannot be excluded that between two observed states more complicated concatenated states, in which the observed principle states alternate in a periodic or aperiodic fashion, exist in U_2 intervals smaller than 0.02 V. For further discussion of this aspect see section 4.2.

Second, along the lower $\phi_{DL,max}$ branches and differently from the upper one, $\phi_{DL,max}$ decreases with decreasing U_2 . If $\phi_{DL,max}$ is smaller than a critical value, a new S-cycle is born. This trend reflects the fact that a lower value of U_2 stabilizes the small hysteresis loop.

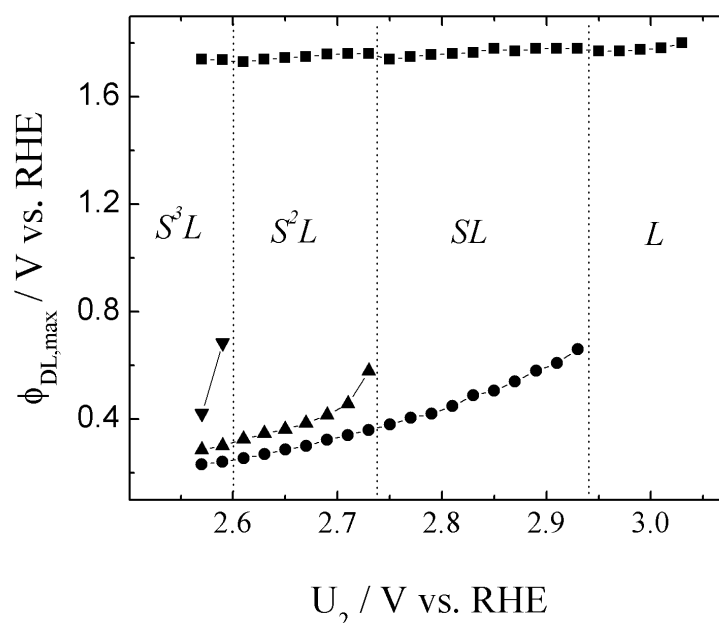


Figure 4.4: Bifurcation diagram showing $\phi_{DL,max}$ (see text) as a function of U_2 for the same experimental conditions as in Figure 4.1.

For a slightly larger H_2SO_4 concentration and thus a smaller uncompensated resistance but identical parameters otherwise, exclusively states with a larger number of S-

cycles than under the previous conditions were observed when decreasing U_2 in 0.01 V steps from the period-1 L-cycle. The low period states from the example discussed above are most likely squeezed to a small range of U_2 values close to the transition to the period-1 L-cycle. Moreover, at this lower cell resistance the behavior was usually not strictly periodic; rather, in most cases the number of S-cycles changed in an aperiodic manner around some mean value. Two examples of complex responses at this higher conductivity are reproduced in Figure 4.5. Figure 4.5 (a) shows an S^5L state, which is, however, not strictly periodic as evident from the time trace of $\phi_{DL,max}$.

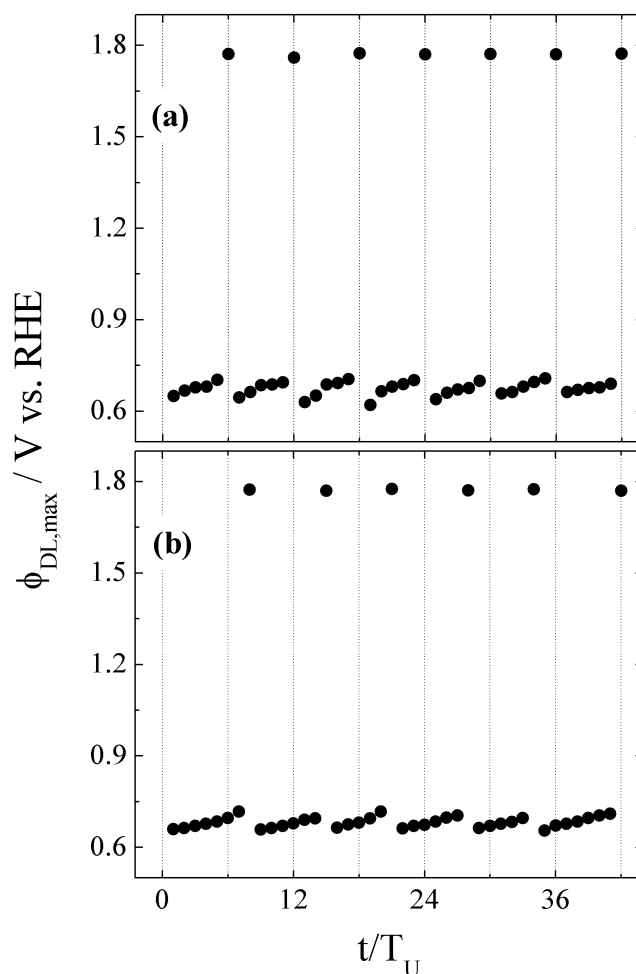


Figure 4.5: (a) S^5L and (b) aperiodic responses during cyclic voltammetry of the the $Pt|H_2SO_4|H_2$ system. Shown is the largest value of the true electrode potential $\phi_{DL,max}$ versus time. (Time is normalized to the period of a voltage cycle, T_u). Positive turning point (a) $U_2 = 2.69$ V, and (b) $U_2 = 2.70$ V. Here, the concentration of H_2SO_4 was 1mM and the uncompensated cell resistance $R_\Omega = 360 \pm 10 \Omega$. The remaining experimental parameters are identical to those in Figure 4.1.

In Figure 4.5 (b) an aperiodic state is depicted, in which the number of S-cycles in between two L-cycles varies between 5 and 7 in an apparently random manner. Upon further lowering U_2 , the average number of S-cycles tended to increase, being 12 at $U_2 = 2.63$ V.

4.2.2 DISCUSSION

The fact that a cyclic voltammogram does not retrace itself during every cycle of the applied voltage but after several cycles implies that the system has some kind of memory to the previous cycle. Such a memory effect arises if there is a process whose characteristic time is of the same order of magnitude as the cycling time and which interacts with at least one of the reaction steps or other processes that occur during a cyclic voltammogram. Hence, the key to understand the complex voltammetric responses lies in identifying this process. Looking at Figures 4.2 and 4.3, it is clear that while the system undergoes S-cycles, the maximum current and also the current at any given value of U are decreasing from cycle to cycle, whereas the activity is reestablished after an L-cycle. This indicates that the process affects the catalytic activity of the electrode with respect to hydrogen oxidation. The increase in the catalytic activity after an L-cycle points to the fact that the essential interaction is through oxide formation or reduction as in reaction step (iv) given above.

As examined in the second chapter, it is well established that Pt-oxide reduction causes a roughening of the Pt surface due to the place exchange process occurring during Pt oxidation. In the present context it is very important that the rough Pt surface resulting from the Pt oxide reduction is known to relax back to its flat state in a rather reversible way, i.e., when keeping the electrode for a sufficient time negative to the potential region, in which oxide formation occurs, the electrode surface flattens again [118, 119]. These two processes, roughening of the surface and its subsequent relaxation, possess exactly the required characteristics underlying the complex voltammetric response. A rougher surface implies a larger surface area and thus a higher current. The healing or flattening of the electrode surface causes a subsequent deactivation. Furthermore, the relaxation is a slow process as shown in cyclic voltammetric experiments in N_2 saturated H_2SO_4 , in which the charge under the hydrogen up peaks decreased during several voltage scans if the electrode potential was kept sufficiently negative, such that Pt oxide did not form [119].

As for the occurrence of high-order periodic voltammetric responses, the following question remains: If the positive turning point is so positive that Pt-oxide can form in one cycle, why does it not form in every cycle? With other words, why does the rougher surface prevent the electrode from being oxidized again at the same value of the applied voltage in the next cycle? At this point, the electrolyte conductivity comes into play. Recall that the maximum true electrode potential, $\phi_{DL,max}$, increases from cycle to cycle while the system undergoes S-cycles and ϕ_{DL} reaches a value, at which the oxidation of the Pt surface sets in when finally an L-cycle is initiated. Hence, it is the larger IR_{Ω} drop through the electrolyte that is associated with the more active surface and takes care that the electrode potential at the positive turning point of the applied voltage stays negative to Pt oxide formation. Only when the relaxation of the surface towards a flat surface is sufficiently advanced and thus the current density has sufficiently decreased, the electrode potential becomes so positive that it enters a potential region, at which the oxidation of the electrode sets in. The large hysteresis loop is then initiated by a self-enhancing feedback mechanism: Since the oxidized surface is inactive for hydrogen oxidation, the initial oxide formation causes a decrease in current density. Owing to the smaller current density, the true electrode potential becomes more positive, and thus the oxide formation becomes faster. In this way, the true electrode potential is driven far into the oxide region. In other words, the oxidation of the Pt electrode leads to a negative differential resistance (NDR) in the stationary (and IR_{Ω} corrected) current-potential curve. An NDR is well known to give rise to the described self-enhancing feedback for a sufficiently large cell resistance (s.a.).

The positive feedback is more pronounced at higher cell resistance R_{Ω} : If the true electrode potential acquires a value, at which oxide formation is about to start, a certain decrease of the current prompts all the more a positive electrode potential the larger R_{Ω} is. Consequently, also oxide formation is accelerated, and thus the current decreases more strongly. This trend offers a plausible interpretation of why complex CVs with a large number of S-cycles in between two L-cycles predominantly in the electrolyte with the higher conductivity were observed.

In summary, the complex voltammetric responses are the result of the interplay between surface roughening owing to the reduction of Pt oxide and the subsequent surface relaxation, on the one hand, and the IR_{Ω} drop through the electrolyte coupled to an NDR, on the other hand. The scheme depicted in Figure 4.6 illustrates this mechanism.

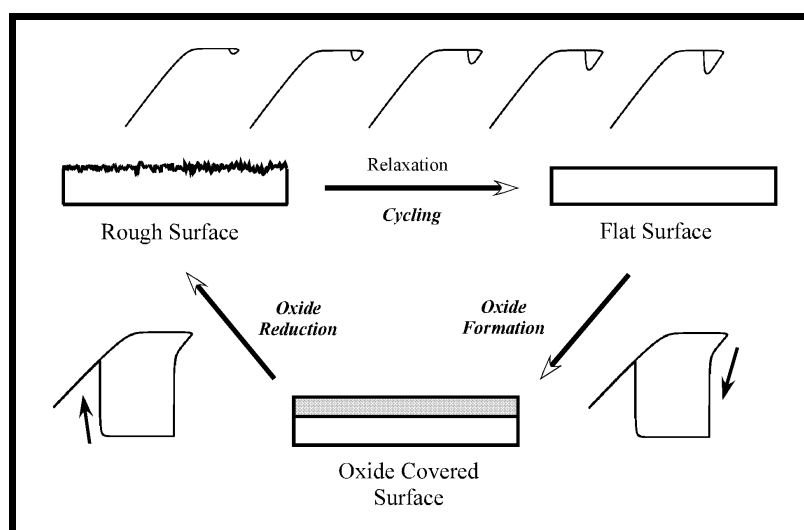


Figure 4.6: Illustration of the interplay between surface activity changes and ohmic drop through the electrolyte leading to the complex voltammetric behavior.

Starting from a rough (high surface area formed just after an L cycle) Pt surface, the reaction current is high, and there is just a very small hysteresis between forward and backward scans. In this case, the double layer potential $\phi_{DL} (= U - IR_{\Omega})$ is very negative with respect to the applied potential, thanks to the IR_{Ω} term. Continuing the cycling, the rough surface starts to relax into a more energetically stable state, and an increase in the peak separation in the I/U curve at high U values is observed. Here, the true working electrode potential (which in its turn is almost identical to ϕ_{DL}) is allowed to go into more positive values driven by the applied voltage due to the smaller values of the ohmic drop, IR_{Ω} . The concomitant decrease in current and the positive potential region excursions of the electrode potential reach a threshold when the electrode surface is flat enough and oxide formation sets in. At this point, an abrupt decrease in I is observed, and ϕ_{DL} and U have almost the same value because of the negligible oxidation current on the oxide covered electrode. After the platinum oxide reduction the surface becomes rough again and the cycle starts anew. Taking as example Figure 4.2 displayed above, the arguments invoking the relaxation of the rough surface towards a flatter state as a cause of the current decrease and the double layer potential increase during the cycling explain the main voltammetric features up to the fourth cycle shown where an L-cycle occurs. Then, as just schematically illustrated in Figure 4.6, the initial, high activity, rough Pt surface is restored during the Pt oxide reduction.

4.3 MODEL AND SIMULATIONS

4.3.1 THE MODEL

The main ideas of the mechanism discussed above can be translated into a mathematical model consisting of a set of ordinary differential equations. The variables of the model are the true electrode potential, ϕ_{DL} , the oxide coverage of the electrode, θ , and the roughness of the electrode surface, r . The latter is defined as the ratio between the actual electrode area, A , and the electrode area of the relaxed (flat) surface, A_0 ; thus, $r \geq 1$.

The evolution equation for ϕ_{DL} is readily obtained from Kirchhoff's law applied to the equivalent circuit of an electrochemical cell as given in chapter 2,

$$C_{sp} \frac{d\phi_{DL}}{dt} = -i_F + \left(\frac{U - \phi_{DL}}{rA_0R_\Omega} \right), \quad (4.1)$$

where constants, variables, and symbols have their usual meaning. According to the above given definition of A_0 and r , r times A_0 is the actual electrode area. The faradaic current density, i_F , is composed of the hydrogen oxidation current density, and the current density due to the formation and reduction of Pt oxide,

$$i_F = -i_H(1 - 0.99\theta) - q_0 \frac{d\theta}{dt}, \quad (4.1a)$$

where q_0 is the charge which flows if one monolayer oxide is deposited on or stripped from an electrode of 1 cm^2 in area. The hydrogen oxidation current density $i_H(1 - 0.99\theta)$ is assumed to instantaneously adjust to variations in ϕ_{DL} and θ . The factor 0.99 takes into account that the observed oxidation current was not identical zero, even on an oxide covered electrode surface. For the sake of simplicity, the dependence of i_H on ϕ_{DL} on the bare Pt surface was modeled by the following equation

$$i_H = b_1 - \frac{b_2}{1 + \exp[b_3(\phi_{DL} - b_4)]}, \quad (4.1b)$$

whereby the constants b_1 , b_2 , b_3 , and b_4 were obtained from a fit to experimental data. Their values are listed in Table 4.1.

Oxide formation and reduction was approximated by the Butler-Volmer-type equation

$$\frac{d\theta}{dt} = k_{\text{ads}}(1-\theta)\exp[\alpha n f(\phi_{\text{DL}} - \phi_{\text{DL},\theta=0.5})] - k_{\text{des}}\theta\exp[-(1-\alpha)n f(\phi_{\text{DL}} - \phi_{\text{DL},\theta=0.5})], \quad (4.2)$$

where k_{ads} and k_{des} represent the adsorption and desorption constants of oxide formation and dissolution, respectively. f stands for F/RT , whereby F , R and T have their usual meanings. α is the transfer coefficient and n represents the number of electrons transferred. $\phi_{\text{DL},\theta=0.5}$ is the potential, at which the electrode is half covered by oxide. Following Angestein-Kozłowska *et al.* [163], the values of k_{ads} and k_{des} were chosen such that the peak separation of the oxidation and reduction current was close to the experimentally observed one.

The ‘heart’ of the model is the evolution of the surface roughness, r , with time, which was described by the following equation

$$\frac{dr}{dt} = K_r k_{\text{des}}\theta\exp[-(1-\alpha)n f(\phi_{\text{DL}} - \phi_{\text{DL},\theta=0.5})] - K_s(r-1). \quad (4.3)$$

The first term in equation (4.3) models the roughening of the surface, which is assumed to be proportional to the desorption rate of the oxide, K_r being a constant of proportionality. The flattening process is described by a simple, potential-independent, relaxation of the rough to the smooth surface with the rate constant K_s .

Finally, the periodic cycling of the externally applied voltage U between two limit points, U_1 and U_2 , can be formally written as

$$\frac{dU}{dt} = \begin{cases} v, U_1 \rightarrow U_2 \\ -v, U_2 \rightarrow U_1 \end{cases}, \quad (4.4)$$

where v is the scan rate, $U_1 \rightarrow U_2$ symbolizes that $dU/dt > 0$ and $U_1 \leq U < U_2$. Accordingly, $U_2 \rightarrow U_1$ means that $dU/dt < 0$ and $U_1 < U \leq U_2$.

The time integration of equations (4.1)–(4.4) was performed with the Livermore solver for ordinary differential equations (lsode) invoking the mode for stiff systems [164]. All parameters, which were not changed in the simulation, are compiled in Table 1. With the exception of K_r and K_s , they were either known from literature or fitted to independent experiments.

Table 4.1. List of symbols (with their meanings, values used in the calculations, and units).

Symbol	Meaning	(Value) Units
k_{ads}	Adsorption constant	(0.1) s^{-1}
k_{des}	Desorption constant	(0.05) s^{-1}
α	Transfer coefficient	(0.5) ---
n	Transferred electrons	(2) ---
θ	Electrode coverage (normalized to the maximum electrode coverage)	---
i_{H}	Hydrogen current density	mA cm^{-2}
i_{F}	Faradaic current density	mA cm^{-2}
I	Current	MA
q_0	Charge that flows when 1 ML of oxide is formed on an electrode of 1cm^2 . ⁷	(0.22) mC cm^{-2}
f	F/RT	(38.92) V^{-1}
C_{sp}	Specific double layer capacitance	(0.02) mF cm^{-2}
R_{Ω}	Uncompensated cell resistance	Ω
U	Applied voltage	V
ϕ_{DL}	Double layer potential	V
$\phi_{\theta=0.5}$	Potential at which $\theta = 0.5$	(0.72) V
U_1	Lower (negative) potential turning point	(0.27) V
U_2	Upper (positive) potential turning point	V
v	Scan rate	(0.1) Vs^{-1}
A_r	Real electrode area	cm^2
A_0	Apparent (geometric) electrode area	(1) cm^2
r	Electrode roughness ($= A_r/A_0$)	---
t	Time	S
T_u	Period of one voltammetric cycle ($= 2(U_2 - U_1)/v$)	S
K_r	Roughening constant	(0.01) ---
K_s	Relaxation or smoothing constant	(0.05) s^{-1}
b_1	Constant in equation (1b)	(6) mA cm^{-2}
b_4	Constant in equation (1b)	(2073) mA cm^{-2}
b_3	Constant in equation (1b)	(22.66) V^{-1}
b_4	Constant in equation (1b)	(0.26874) V

⁷ It was assumed that per Pt atom two electrons are involved in the oxidation process (see equation (4.3) and the value for n in this Table). Thus, the value chosen for q_0 implies that the maximum oxide coverage which completely inhibits hydrogen oxidation is 0.5. It was confirmed that also for a maximum oxide coverage of 1, and thus $q_0 = 440\text{ mC cm}^{-2}$, the same qualitative trend as reported here occurs. However, the absolute values of U_2 at which a particular behavior is found is shifted towards larger values; in addition, the bifurcation fine-structure might be slightly altered.

4.3.2 SIMULATIONS AND DISCUSSION

Integrating equations (4.1)–(4.4) reveals that this set of equations indeed possesses high-order periodic and aperiodic solutions, which bare all the properties of the experimentally observed complex cyclic voltammetric responses for realistic values of the parameters. Note, however, that smaller values for the cell resistance were used in the calculations than in the experiments since for realistic values the problem was so stiff that it was difficult to handle numerically.

In Figure 4.7 (a) the voltammetric response is depicted, whereas Figures 4.7 (b)–(e) show the temporal change of the externally applied voltage, the surface roughness, the oxide coverage of the electrode and the true electrode potential, respectively. Clearly, the calculated cyclic voltammogram exhibits the same basic features as the experimentally obtained period-3 response shown in Figure 4.1 (c), namely a periodic behavior composed of two small hysteresis loops followed by a large hysteresis loop. Furthermore, for potentials close to U_2 , the current density is smaller in the second S-cycle than in the first one. This feature is particularly pronounced on the negative scan in both experiments and simulations. However, on the positive voltage scan it is more pronounced in the experiments than in the simulations. This small discrepancy probably results from the value chosen for the constants determining surface roughening and flattening, K_r and K_s . Since equation (4.3) represents only a crude approximation to the roughening process, these constants, which are not available from the literature, were only roughly adjusted to the observed time scales, and no attempt was made to quantitatively match the experimental behavior. Two other discrepancies between the experimental and simulated CVs are apparent: First, in the experiments the mass transport limited current region exhibits a small decrease when going to positive potentials, which is not the case in the simulation. This is a result of the chosen function (equation (4.1b)) used to model the hydrogen current, where the fit to the experimental data exhibited a small discrepancy in this potential region. The second dissimilarity is the residual current after the oxide formation, which is seen in the experiment but is not reproduced in the calculations. As discussed above, this current is due to the oxygen evolution reaction. For the sake of simplicity, the latter was not included in the model.

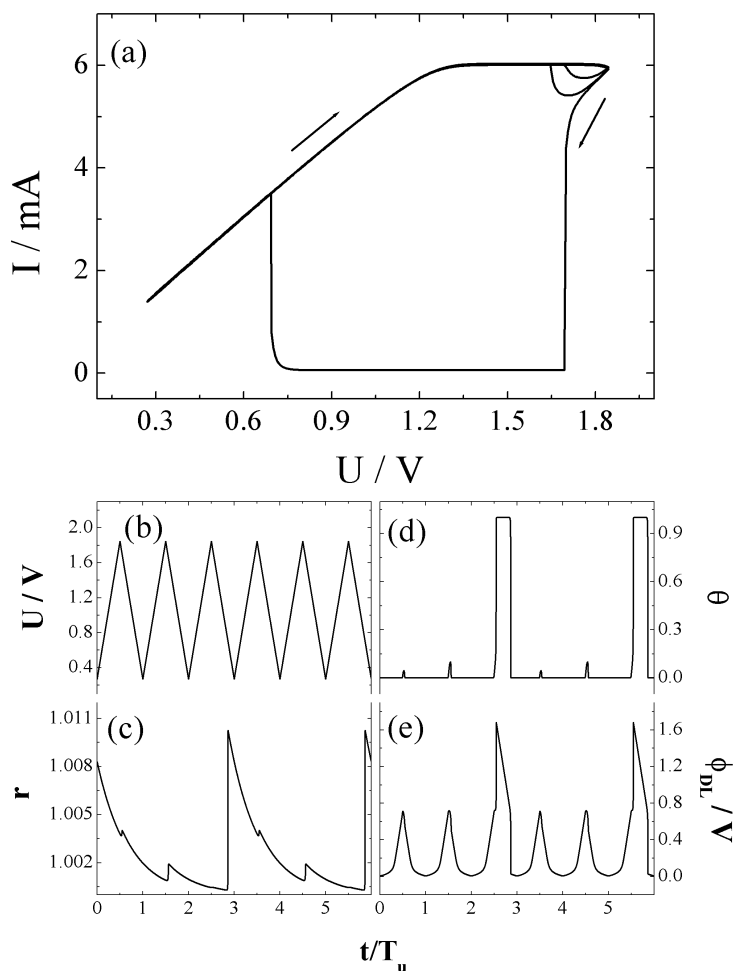


Figure 4.7: (a) Calculated period-3 (S^2L) voltammetric response and corresponding time series of (b) U , (c) r , (d) θ , and (e) ϕ_{DL} . T_u period of the cycling voltage. $R_{\Omega} = 190 \Omega$ and $U_2 = 1.8445 \text{ V}$, the remaining parameters are given in Table 4.1.

To obtain a better picture of the dynamics it is instructive to follow how the variables change in the course of this period-3 response (Figure 4.7 (b)–(d)). As apparent from Figure 4.7 (c), the surface roughness increases jump-like when going from the oxide covered to the bare Pt electrode and essentially relaxes during the three subsequent voltage cycles to its original value. This relaxation is slightly disturbed when the minor oxide coverage, which forms during the S-cycles (cf. Figure 4.7 (d)), is reduced. Thus, the relaxation phase is modulated with the cycling period. It is remarkable that the changes in the surface roughness are only on the order of 1 %, which means that minor changes in the electrode area that are very hard to detect experimentally suffice to induce the complex voltammetric response. Figures 4.7 (d) and (e), in which the changes of the oxide coverage and the true electrode potential are shown, confirm the picture developed above, namely that an increasing oxide

coverage goes along with an increasing value of ϕ_{DL} (although the latter one is not as pronounced as in the experiments and is not evident in the scale of the figure).

Another example of a simulated period-3 complex response constitutes the SL^2 state and is given in Figure 4.8 for a U_2 value higher than that used in Figure 4.7 and the same remaining conditions. The main feature of this set of SL^2 response, when compared to the S^2L depicted in Figure 4.6, is the fact that here two large excursion cycles are necessary to restore the initial high activity.

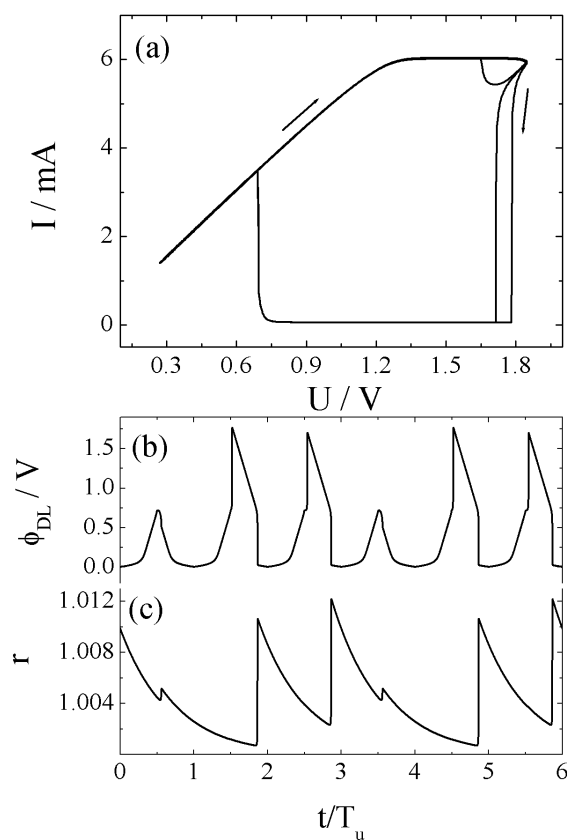


Figure 4.8: (a) Calculated period-3 (SL^2) voltammetric response and corresponding time series of (b) ϕ_{DL} , and (c) r . $R_{\Omega} = 190 \Omega$ and $U_2 = 1.8485 \text{ V}$, the remaining parameters are given in Table 4.1.

When varying U_2 while keeping constant all other parameters used to produce Figures 4.7 and 4.8, a very large variety of complex cyclic voltammetric responses were found, including aperiodic states as well as responses where the number of S-cycles in between two L-cycles alternates. Examples of SL , SL^2 and S^2LS^6L states are given in Figure 4.9 in terms of the voltammetric response and the coverage time series.

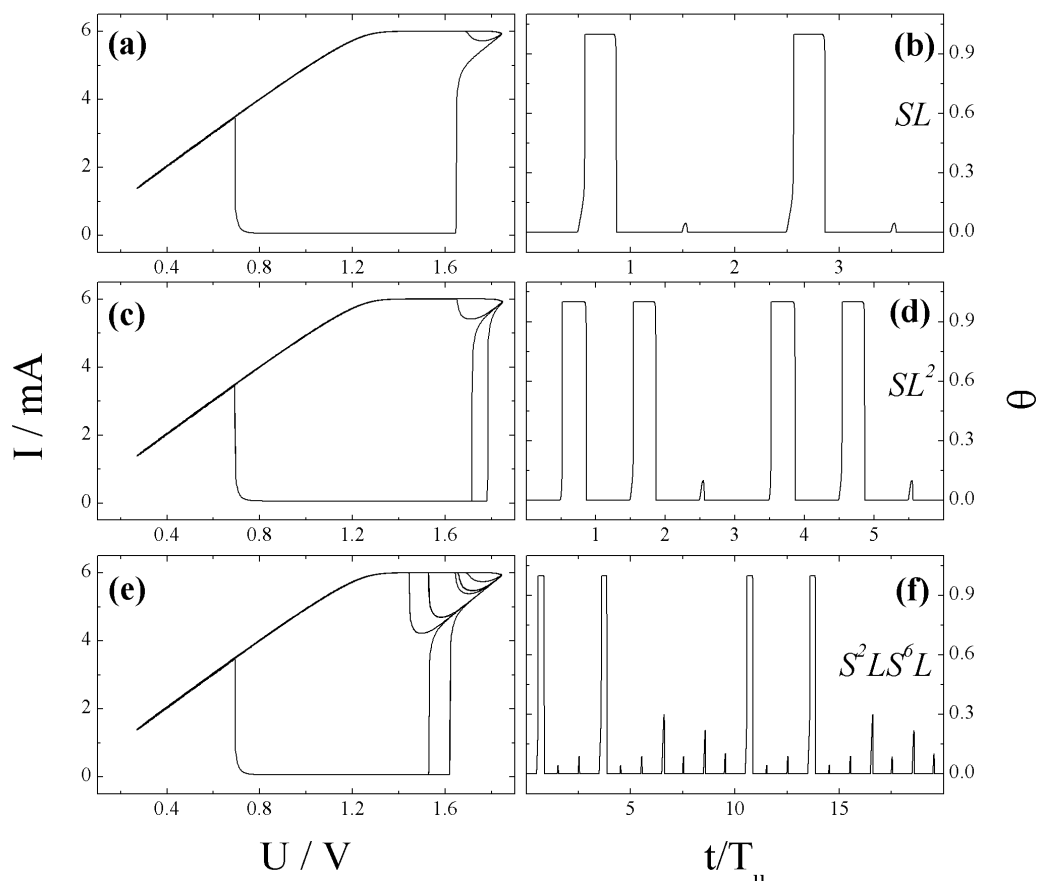


Figure 4.9: (a) Calculated period-2 (SL) voltammetric response and (b) corresponding time series of θ for $U_2 = 1.844900$ V. Period-3 (SL^2) (c) voltammetric response and (d) corresponding time series of θ for $U_2 = 1.848500$ V. Mixed mode (S^2LS^6L) (e) voltammetric response and (f) corresponding time series of θ for $U_2 = 1.844303$ V. In all plots $R_\Omega = 190 \Omega$, and the remaining parameters are given in Table 4.1.

An overview of the obtained dynamics is depicted in Figure 4.10. Note that in this figure the abscissa is strongly nonlinear since some of the states existed only in tiny parameter intervals, whereas other states occurred in large regions of U_2 . Representative values of U_2 , for which the respective behavior was observed, are compiled in Table 4.2. Figure 4.10 exhibits some general features and trends that are independent of the special parameter sets used in the calculations. First, the U_2 range of complex responses is encircled by period-1 CVs of the small hysteresis-type to the low-potential end, and period-1 CVs with large hysteresis loops at the high potential end. When increasing U_2 from the period-1 S-cycle, the S-cycles are at first only seldom interrupted by an L-cycle, then more and more often until L- and S-cycles take turn in the period-2 SL state. Upon further increasing U_2 , two

S-cycles are now separated by several L-cycles, whereby the number of L-cycles increases until the threshold is reached, at which the period-1 L-response exists.

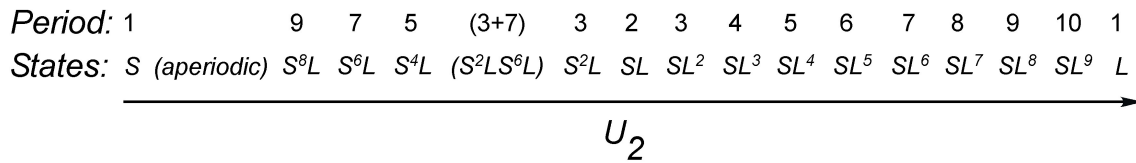


Figure 4.10: Different dynamic states observed upon decreasing U_2 from the L^1 -state. $R_\Omega = 190 \Omega$, the remaining parameters and the numerical values for U_2 , at which the respective states existed, are given in Table 4.1 and Table 4.2, respectively.

Table 4.1. Typical U_2 values for the states described in Figure 4.10. $R_\Omega = 190 \Omega$, Other parameters as given in Table 4.1.

U_2 / V	Observed states
< 1.84426	P1 – S
1.844293	(aperiodic)
1.844294	P9 – S^8L
1.844295	P7 – S^6L
1.844297	P5 – S^4L
1.844303	(S^2LS^6L)
1.844304	P3 – S^2L
1.844900	P2 – SL
1.848500	P3 – SL^2
1.848900	P4 – SL^3
1.849000	P5 – SL^4
1.849010	P6 – SL^5
1.849020	P7 – SL^6
1.849022	P8 – SL^7
1.849025	P9 – SL^8
1.849026	P10 – SL^9
> 1.849035	P1 – L

Looking only at the right part of the diagram shown in Figure 4.10 one could get the impression that upon decreasing U_2 only states SL^n exist whereby n decreases from ∞ to 1 as U_2 decreases. A further decrease of U_2 would then naturally reverse this sequence, producing S^nL states with n increasing from 1 to ∞ . However, as apparent from the left part of Figure 4.10, this picture is too simple. Rather, in some calculations in between two such base states, concatenated states which partly existed only in tiny parameter intervals were detected. For

the present set of parameters, such a state is, e.g., the S^2LS^6L state. Furthermore, aperiodic states, in which the number of S states in between two L states alternated in an apparently random manner around an average number, similar to observations in the second set of experiments at higher conductivity were found (cf. Figure 4.7 (b)). These observations suggest that the complete bifurcation diagram is as complicated as those found for so-called mixed-mode oscillations [165].⁸

The existence of the aperiodic and concatenated states also evidences that the complex responses cannot be explained by a linear superposition of two time scales, the cycling period and the relaxation time. Rather, the dynamics is the result of the coupling between the forcing period of U and nonlinearities in the evolution equations. As discussed above, at low ionic strength the decrease of current density owing to oxide formation gives rise to a self-enhancing ('autocatalytic') growth of the (true) electrode potential, which causes the system to be bistable under stationary conditions: In a certain range of U, the system can either be in an 'active' state where hydrogen oxidation proceeds on the bare Pt surface with a high rate or in a passive state, in which the electrode surface is covered by oxide and the current density is low. Thus, from a dynamical point of view the problem discussed here is described as a periodically forced bistable system.

Some (though not extensive) tests were done to check whether the complex responses also exist if it is assumed that Pt oxide does not inhibit the reaction, i.e., with equations (4.1)–(4.4) where in equation (4.1a) the term $(1 - 0.99\theta)$ was omitted. This removes the positive feedback loop in the system. In the simulations only period-1 CVs were obtained which points to the fact that the autocatalysis is indeed necessary for the occurrence of the complex, nonlinear behavior.

In calculations with a smaller cell resistance, S^nL -periods with n larger than in Figure 4.10 were obtained easily, whereas the highest SL^n -states of the above simulations were not detected. Besides, the relative ΔU_2 -interval⁹ in which S^nL -states existed was larger at higher conductivity. This is the same trend which was observed in the experiments (cf. Figures 4.1 and 4.5) and which becomes plausible when considering the fact that the positive feedback is

⁸ Mixed-mode oscillations are periodic or aperiodic oscillations which are composed of different numbers of small and large amplitude oscillations [24, 125, 166].

⁹ U_2 at the border to the S^1 -response - U_2 in the middle of the interval in which SL -cycles exist normalized to the total U_2 interval in which complex CVs were detected.

weaker at higher conductivity (s.a.). In addition, in the simulations with a higher conductivity complex dynamic behavior existed which was only composed of S-cycles for values of U_2 that were lower than the one at which the first L-cycle appeared. In Figure 4.11 a bifurcation diagram is shown in which the maximum values of θ during each period of the voltage cycling is plotted versus U_2 . Note that θ_{\max} is considerably smaller than 1 throughout, whereas it would be close to 1 in an L-cycle. The bifurcation diagram is typical for a period-doubling cascade to chaos [167-169].

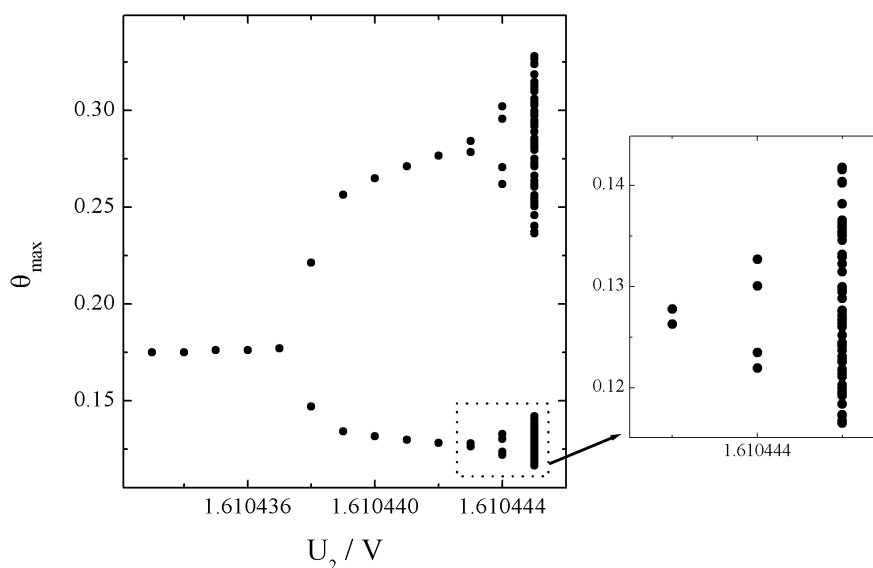


Figure 4.11: Calculated bifurcation diagram for $R_{\Omega} = 150 \Omega$. The remaining parameters are given in Table 4.1.

The next maximum map depicted in Figure 4.12 has (with the exception of one point) a unimodal shape as typical for chaos arising through the Feigenbaum scenario. This behavior is a further manifestation that nonlinearities in the evolution laws are decisive for the complex voltammetric responses. Furthermore, they demonstrate that even the exclusive formation and dissolution of oxide in the submonolayer region which bring about only a minor roughening of the surface suffice to induce complex behavior.

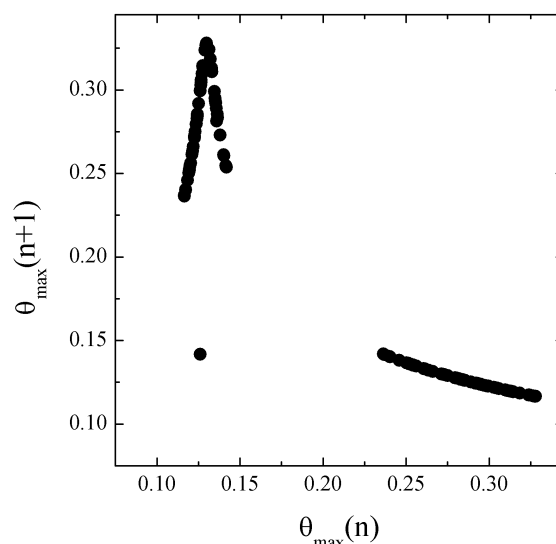


Figure 4.12: Next maximum map for the data shown in Figure 4.11 at $U_2 = 1.610445$ V.

4.4 GENERAL DISCUSSION

According to the considerations above, the essential ‘ingredients’ necessary to cause higher periodic and aperiodic cyclic voltammograms are: (a) A faradaic reaction that is inhibited by oxide formation on the electrode and thus generates an NDR in the polarization curve at positive potentials; (b) a non-negligible ohmic drop through the electrolyte which together with the NDR gives rise to a positive feedback in the electrode potential; (c) a roughening of the electrode surface due to oxide reduction and its subsequent relaxation to a flat surface, whereby the relaxation has to occur on a time scale which is at least of the order of the voltage cycling period.

These conditions are fulfilled by different noble metal electrodes, whereby Pt and Pd are probably the most important ones, and a large variety of oxidation reactions, in particular the electrocatalytic oxidation of small organic molecules, such as formic acid, aldehydes or alcohols. This suggests that also the large variety of complex cyclic voltammograms reported by Schell and coworkers [152-159] are brought about by this principle mechanism. One criterion, which these results should then satisfy, is that the complex responses should disappear when the ohmic drop is negligible. Zdraveski *et al.* [159] investigate the impact of the uncompensated resistance in two sets of experiments. In one set the cell resistance is changed by varying the position of the RE, in the other one by variation of the supporting electrolyte (sodium hydroxide) concentration. Starting from a period-2 response, in both sets of experiments a decrease in the uncompensated cell resistance, R_{Ω} , eventually leads to

period-1 behavior. Thus, the authors concluded ‘ R_{Ω} cannot be eliminated from playing a role in the cause of instability...’ [159], which is in accordance with the presented conjecture.

As mentioned in the introduction, complex voltammetric responses were also observed during Cu dissolution in acidic solution [160]. It seems to be conceivable that also here the same principle mechanism is operative: Upon the increase of the electrode potential the ‘active’ dissolution of Cu is hindered due to the passivation of the Cu surface which is caused by its oxidation. Hence, the polarization curve possesses an NDR. Furthermore, it appears to be likely that reduction of the oxide goes also along with roughening and subsequent healing of the surface. This example demonstrates how manifold the reactions might be, in which roughening/relaxation of the electrode surface coupled to an NDR causes dynamic instabilities of CVs.

So far the basic features that give rise to complex cyclic voltammetric responses have been stressed. However, different bifurcation scenarios between the period-1 S- and L-cycles as a function of U_2 were observed in different reactions and also for different experimental conditions in one reaction (see e.g. [158]). In view of this manifold of different dynamic states observed, it is natural to ask for the causes of these differences. At this point, it is important to note that the detailed route through the U_2 window of complex response depends sensitively not only on the value of parameters that do not affect (at least in zeroth order) the electrode kinetics (such as the conductivity, where the correct trend could be reproduced in the simulations) but also on details of the reaction mechanism, and thus on the specific electrochemical reaction under investigation. Furthermore, the relaxation process will be in general potential dependent and can be altered by adsorbates. E.g., it is known that Cl^- ions enhance the mobility of adatoms on gold surface and lead to chemical annealing [72, 170-172], other adsorbed species will reduce the rate of relaxation. All these aspects will determine the intricate bifurcation fine structure. Thus, the presented explanation of the occurrence of high-order periodic or aperiodic CVs should not be understood as being exhaustive. Rather, it gives a minimum skeleton, which can give rise to complex voltammetric responses of the desired type and is the primary reason for dynamic instabilities in cyclic voltammograms in many electrochemical reactions.

Besides these aspects, one should be aware of another assumption implicitly made so far, namely that spatial variations can be neglected. But it is known that oxide formation proceeds through a nucleation and growth mechanism[41]. In fact, it was possible to measure

the potential distribution along the ring electrode during cyclic voltammetry, and the transition from the free Pt electrode to Pt oxides was found to occur on the electrode even on a mm scale never completely homogeneously. In some voltage cycles the entire electrode became even never completely covered by oxide. Rather, an oxide area expanded along the ring until the electrode was approximately half covered by it. Successively, it shrank again. In the cyclic voltammogram, these (rather rare) occurrences manifested themselves in current-potential curves, in which the current decreased to approximately half of its highest value, the entire cycle resembling neither a typical S- nor a typical L-cycle. It is remarkable that also in the studies by Schell and coworkers such intermediate cycles are sporadically reported (see, e.g., Figure 1 (b) in ref. [159]).

One example of the spatial dependence of the oxide formation during the cycling is illustrated in Figure 4.13. In the first plate, Figure 4.13 (a), a period-3, S²L cyclic voltammogram is depicted. Here, U_2 value was set to 2.73 V and the remaining conditions as given in Figure 4.1 above. The region around the U_2 value, i.e., the ‘interesting’ region concerning the oxide formation along the ring, is investigated through the I and U_{PP} plots in a neighborhood region of U_2 in Figure 4.13 (b) and (c), respectively. The applied voltage U is also depicted in Figure 4.13 (b). In these plots, the time was set to zero at the beginning of each cycle. Furthermore, these curves were numbered in terms of their sequence in which they appear during the cycling. The first set of I and U_{PP} profiles, curves 1 in Figures 4.13 (b) and (c), illustrates the behavior near U_2 for the smaller hysteresis cyclic voltammogram. From the U_{PP} signal (curve 1 in Figure 4.13 (c)) it is clear that the electrode remains outside the oxide region and no electrode blocking is observed, as further evidenced in curve 1 in Figure 4.13 (b) where the current remains at high values close to the U_2 limit. Moreover, as shown in curve 1 in Figure 4.13 (c), the amplitude of U_{PP} remains around 0.07 V and reflects the inhomogeneous catalytic activity along the ring upon the hydrogen electrooxidation reaction. The subsequent cycle is the one with a slightly larger hysteresis in the I/U curve (curves 2 in Figures 4.13 (b) and (c)). Quite differently from the behavior shown in the first cycle, the U_{PP} signal shows an increase in amplitude up to about 0.27 V during the backward scan. At this point, U_{PP} values of 0.63 and 0.90 V are found at different positions along the ring, evidencing the coexistence of free and oxide covered of regions, respectively. Finally, in the third voltammetric cycle, a large hysteresis cycle, L, the complete transition from free to oxide covered Pt is observed in the vicinity of U_2 . Such a transition does not occur homogeneously, it rather occurs through a nucleation and growth mechanism [41]. This can

also be seen in the U_{PP} plots (curve 3 in Figure 4.13 (c)) at around 23.5 s, where the amplitude amounts to ca. 0.38 V. The amplitude in the U_{PP} signal during the transition can be interpreted as the result of the different oxidized states transiently distributed along the ring.

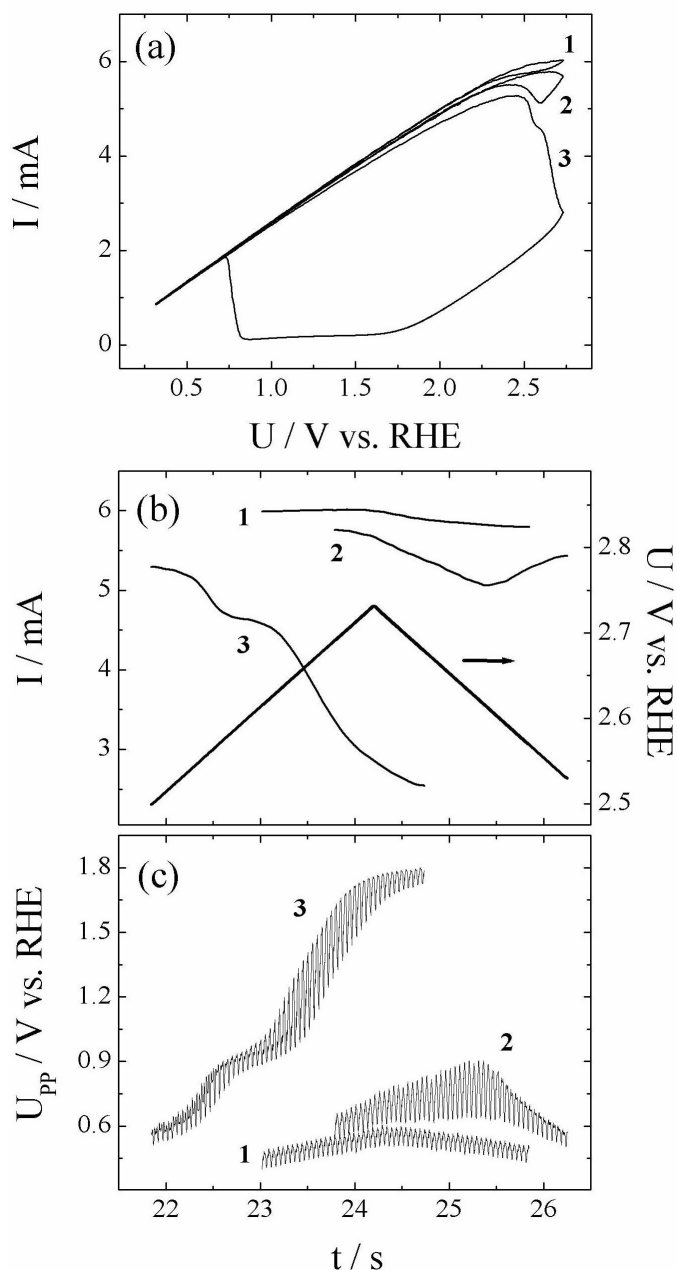


Figure 4.13: (a) Period-3, S^2L , cyclic voltammograms. (b) Current close to the positive turning point, U_2 , value and the applied voltage U as a function of time. (c) Corresponding interfacial potential U_{PP} vs. time for each current series displayed in (b). $U_2 = 2.73$ V. The remaining conditions are as those given in Figure 4.1.

Since the experiments just described in Figure 4.13 were carried out using a sampling rate of 1 kHz for measuring the potential close to the Pt ring with the micro probe, it is

possible to reconstruct the U_{PP} distribution with 50 points/rotation resolution along the Pt ring. Figure 4.14 depicts the three-dimensional plots of U_{PP} as a function of time and ring position for the data shown in Figure 4.13 (c). Curves 1, 2 and 3 in Figure 4.13 (c) are displayed in Figure 4.14 (a), (b), and (c), respectively.

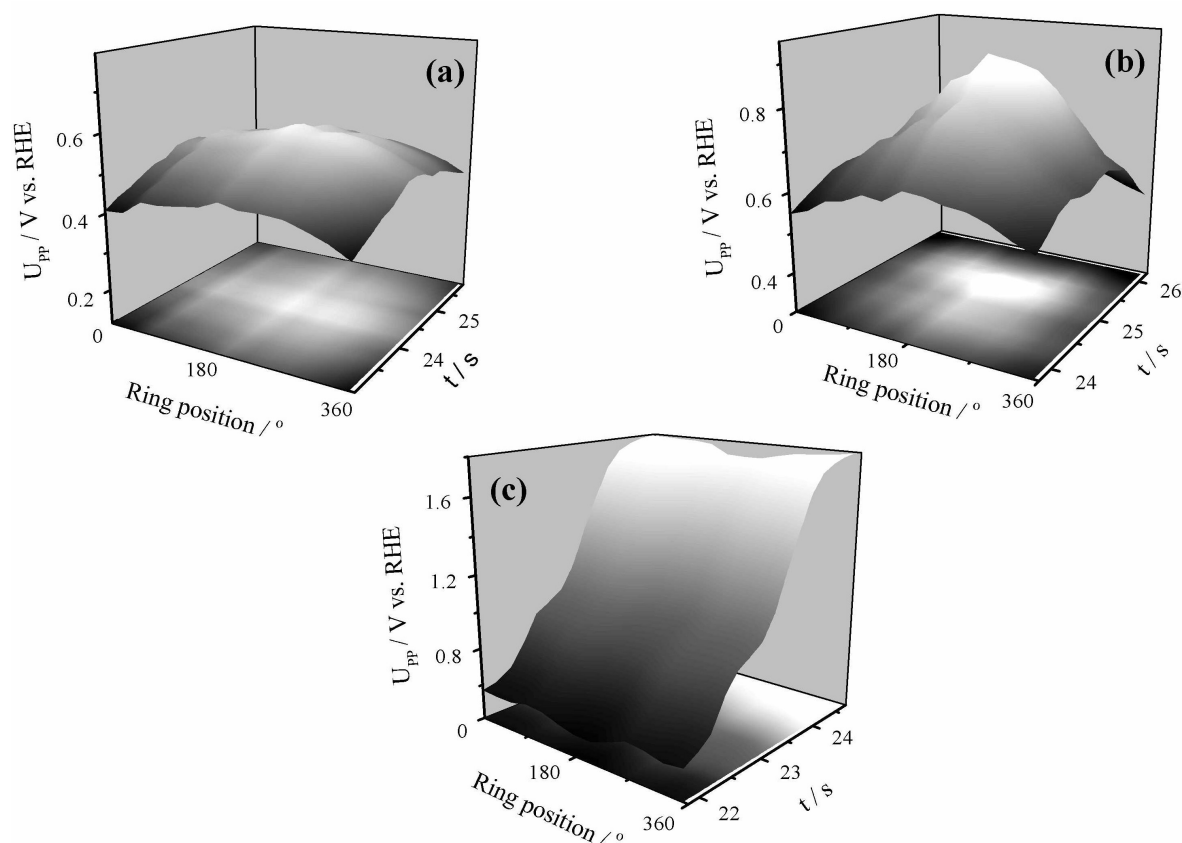


Figure 4.14: Three-dimensional representation of U_{PP} as a function of time and ring position for curves (a) 1, (b) 2, and (c) 3 as shown in Figure 4.13 (c).

This figure, supports the discussion given above. In the first cycle, the U_{PP} distribution around U_2 (Figure 4.14 (a)) can be roughly considered homogeneous and no appreciable differences in the U_{PP} distribution along the ring is observed. On the other hand, significantly inhomogeneous U_{PP} distribution is observed during the second cycle, as illustrated in Figure 4.14 (b). As can be seen, the oxide blocks mainly the center of the Pt ring, i.e., the arbitrarily identified, region around 180° , whereas the opposite region at 0 and 360° remains oxide free and, consequently, active for the hydrogen electrooxidation reaction. The mentioned transition from free Pt (low U_{PP}) to Pt oxide (high U_{PP}) during the third cycle is depicted in Figure 4.14 (c). As stated above, such a transition, in fact, proceeds in an inhomogeneous manner. However, due to the wide potential range visited during the transition such

inhomogeneous states (regions separated by ca. 0.38 V along the ring) are not clearly observable in this representation. This feature is better visualized when plotting only the inhomogeneous part of U_{PP} ($= U_{PP} - \langle U_{PP} \rangle_x$), as done in Figure 4.15.

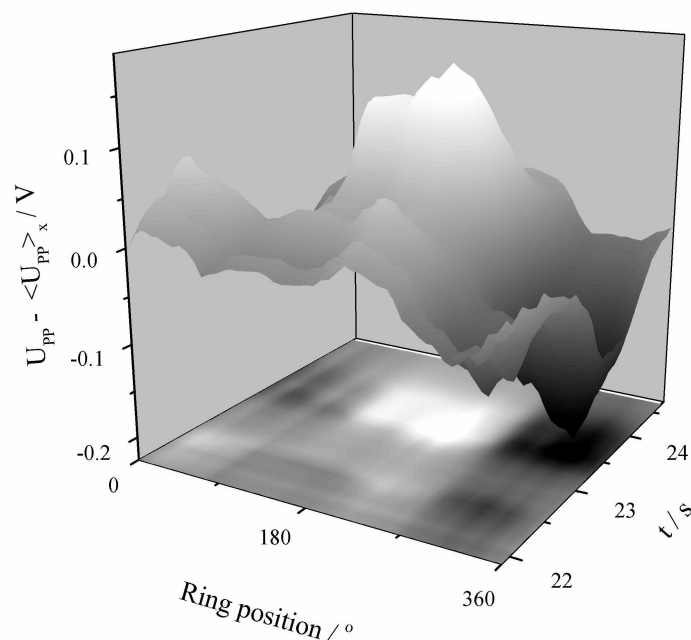


Figure 4.15: Three-dimensional representation of the inhomogeneous part of the interfacial potential, $U_{PP} - \langle U_{PP} \rangle_x$ as a function of time and ring position for the data shown in Figure 4.14 (c).

Hence, the main importance of the oxide formation along the ring electrode is the fact that except for very small electrodes, the transition from the free to the oxide covered surface proceeds in an inhomogeneous manner also on a macroscopic scale.

4.5 CONCLUDING REMARKS

The occurrence of complex cyclic voltammograms implies that there is a slow process with a characteristic time on the order of the period of the cycling voltage that interacts with the remaining electrochemical steps. The relaxation of a rough surface, which is generated when an oxidized electrode surface is reduced to a smooth surface, has been identified as such a process. Surface roughening and healing is most likely an essential step in all of the so far reported complex voltammetric responses.

Further essential features are (a) that an oxidation reaction proceeds more slowly on the oxidized than on the bare electrode surface, i.e., that the polarization curve possesses a region of negative differential resistance and (b) that there is a non-negligible ohmic potential drop through the electrolyte. The latter is often the case even for small cell resistances since the reaction rate easily takes on considerable values at potential values close to the onset of oxide formation.

The derived conditions are general and hold under many experimental situations, suggesting that complex voltammetric responses are no exotic phenomena but exist for a large variety of electrode reactions and electrode materials.